Journal of Geoscience and Environment Protection, 2025, 13(11), 88-110
https://www.scirp.org/journal/gep
ISSN Online: 2327-4344
ISSN Print: 2327-4336

Petrographic Characteristics and Pore Structure Analysis of Benxi Formation Sandstone Reservoirs in the Yanchuan East Block, Ordos Basin

Qiyu Gao, Meng Wang, Tianchao Guo, Xiao Yang

Yan'an Gas Field Gas Production Plant No. 5, Shaanxi Yanchang Petroleum (Group) Company Limited, Yan'an, China
Email: 1878003711@qq.com

How to cite this paper: Gao, Q. Y., Wang, M., Guo, T. C., & Yang, X. (2025). Petrographic Characteristics and Pore Structure Analysis of Benxi Formation Sandstone Reservoirs in the Yanchuan East Block, Ordos Basin. *Journal of Geoscience and Environment Protection, 13,* 88-110.
https://doi.org/10.4236/gep.2025.1311006

Received: October 4, 2025
Accepted: November 16, 2025
Published: November 19, 2025

Abstract

This study investigates the Benxi Formation sandstone reservoirs in the Yanchuan East Block of the Ordos Basin, employing an integrated approach that includes core observation, thin-section analysis, scanning electron microscopy, high-pressure mercury intrusion, and petrophysical testing to systematically evaluate reservoir petrographic features and pore structures. Results reveal that Benxi Formation sandstones predominantly comprise quartz sandstones, lithic quartz sandstones, and lithic sandstones, characterized by high quartz content, widespread volcanic lithic fragments, moderately well-sorted grains, and complex cement types. Pore types are dominated by residual intergranular and dissolution pores, with minor intracrystalline pores and fractures; overall porosity ranges from 0.17% to 9.07% (average 4.74%), and permeability from 0.01 to 6.05 mD, classifying them as ultra-low porosity and tight reservoirs. High-pressure mercury intrusion indicates microfine throats as the primary structure, divisible into four distinct types. Diagenetically, compaction and cementation are the main drivers of primary pore loss and reservoir tightening, whereas late-stage dissolution partially ameliorates pore networks. Overall, Benxi Formation sandstone reservoirs exhibit pervasive densification but localized favorable pore assemblages and connectivity, facilitating hydrocarbon migration and accumulation. These findings advance understanding of Upper Paleozoic tight sandstone reservoir characteristics and aid in predicting sweet spots.

Keywords

Ordos Basin Yanchuan East Block, Benxi Formation, Sandstone Reservoir, Petrographic Characteristics, Pore Structure, Diagenesis

1. Introduction

Tight sandstone reservoirs, as a critical component of unconventional oil and gas resources, have garnered significant global attention due to the declining availability of conventional resources (Abdulhadi et al., 2025; Caineng et al., 2010; Wang et al., 2016; Zou et al., 2015). Countries like the United States and Canada have achieved large-scale production through advancements in understanding reservoir genesis, pore structures, diagenesis, and engineering techniques such as horizontal drilling and hydraulic fracturing (Leary et al., 2020; Meissner & Thomasson, 1999; Whalen & Day, 2010). In China, progress in basins like Ordos, Sichuan, and Songliao has uncovered substantial tight gas accumulations, with the Ordos Basin's Upper Paleozoic reservoirs emerging as a key pillar for natural gas output (Jia et al., 2022; Li et al., 2020; Liu, 2023; Wang & Li, 2024; Yang et al., 2005; Zhao et al., 2024). The Yanan Gas Field in the southern Ordos Basin exemplifies this potential, where Carboniferous-Permian tight sandstones demonstrate economic viability.

The Benxi Formation, a lower Carboniferous unit in this field, features a barrier island-lagoon depositional system influenced by marine transgressions and regressions, resulting in complex facies distributions (Li et al., 2025b; Li et al., 2023; Meng et al., 2024; Xu et al., 2021). Sand bodies in nearshore and barrier island settings exhibit high quartz content, diverse cements, and volcanic lithics, providing a foundation for reservoirs. However, intense compaction, cementation, and burial have densified these rocks, while late dissolution and fracturing create localized high-quality zones enabling hydrocarbon migration and accumulation. Despite extensive global and domestic research on tight sandstones—emphasizing diagenetic controls, pore-throat characteristics, and accumulation models (Hu et al., n.d.; Li et al., 2025c; Liu et al., 2015; Wang et al., 2019; Xi et al., 2015b; Zou et al., 2013)—studies on the Benxi Formation remain limited. Prior work has focused on sequence stratigraphy and depositional environments, with insufficient detail on lithology, pores, throats, and diagenesis, impeding insights into entrapment and favorable reservoir prediction.

This study addresses this gap by targeting Benxi Formation sandstones in the Yanchuan East Block, using core observation, thin-section identification, cast thin-section analysis, scanning electron microscopy, high-pressure mercury injection, and petrophysical testing. It delineates lithological attributes and provenance via core/thin-section analyses; identifies pore evolution through microscopy; classifies throats using mercury/petrophysical data; and examines diagenetic impacts on densification and enhancement. These efforts summarize reservoir characteristics and evolution, providing a basis for efficient exploration in the Yanan Gas Field and advancing theories on tight sandstone reservoirs in China.

2. Geological Background

2.1. Regional Geological Overview

The Ordos Basin, located in northwestern China, forms part of the North China

Craton and represents a multi-cycle sedimentary basin spanning from the Paleozoic to the Mesozoic eras (Gao & Wang, 2017; Liu et al., 2024; Pan et al., 2024). The basin exhibits an approximately square shape, covering about 370,000 km^2, with well-defined boundaries: it borders the Yinshan Orogenic Belt to the north, the Qilian Orogenic System to the west, the Qinling Orogen to the south, and the Taihang Uplift to the east. Structurally, the basin interior is generally stable, dominated by gently dipping monoclines, with localized development of faults and anticlinal structures. The sedimentary cover is thick, featuring widespread Paleozoic, Jurassic, and Cretaceous deposits, establishing the basin as one of China's premier hydrocarbon accumulation regions. The Yanan Gas Field lies within the Yishan Slope in the southern basin, where the structural framework is simple, faults are sparse, and depositional continuity is favorable, providing an optimal geological setting for the formation of Upper Paleozoic tight sandstone gas reservoirs.

2.2. Sedimentary and Stratigraphic Characteristics of the Yanchuan East Block

The Yanchuan East Block exhibits complete stratigraphic development, with exposed strata ranging from the Ordovician to the Cenozoic (Greentree et al., 2006; Kuang et al., 2020; Xiong et al., 2024; Zhang et al., 2022). The Carboniferous–Permian succession attains significant thickness and constitutes the primary target for hydrocarbon exploration and development. Carboniferous deposits are widespread, encompassing the Taiyuan and Benxi Formations, characterized by interbedded sandstones, mudstones, and limestones, with localized coal seams. The Permian includes the Shanxi, Shihezi, and Shiqianfeng Formations, featuring interbedded sandstones, siltstones, and mudstones in diverse depositional environments that reflect distinct marine-terrestrial transitional facies. Within the study area, the Benxi Formation occupies the lower Carboniferous, with thicknesses typically ranging from 40 to 80 m. Its lithofacies are dominated by sandstones, interbedded with minor mudstones and limestones, and it developed within a barrier island-lagoon depositional system. Overall, the stratigraphic succession in the Yanchuan East Block is continuous, with stable sandstone body distributions, offering advantageous conditions for investigating reservoir characteristics.

2.3. Depositional Environment and Provenance of the Benxi Formation

The Benxi Formation formed during the Late Carboniferous, influenced by transgressive–regressive cycles that engendered a complex and variable depositional environment, primarily featuring a barrier island–lagoon system (Gao & Wang, 2017; Li et al., 2023; Meng et al., 2024; Xu et al., 2021; Zhao et al., 2024). Barrier island sand bodies exhibit high depositional energy, dominated by quartz sandstones with moderate to well-sorted grains and high roundness. In contrast, lagoonal settings are characterized by siltstones and mudstones, with localized thin coal seams. Provenance primarily derives from paleo-uplifts in the northern and northeastern basin margins, supplying predominantly quartz and volcanic lithic

fragments, which provided the material foundation for reservoir formation. Variations in depositional processes and provenance conditions account for the diversity in lithological composition, grain size characteristics, and pore structures of Benxi Formation sandstones, while establishing the groundwork for subsequent diagenetic processes and reservoir evolution.

3. Reservoir Lithological Characteristics

The Benxi Formation was deposited in a barrier island–lagoon environment. Core observations from sampled wells indicate that, due to wave and tidal reworking and sorting, quartz content is high, and lithofacies quality is relatively favorable (Congxian & Ping, 1991; Xu et al., 2021). The primary reservoir sandstones comprise quartz sandstones, lithic quartz sandstones, and lithic sandstones, among which quartz sandstones account for approximately 58.1%, lithic quartz sandstones for 26.7%, and granitic lithic sandstones for 15.1% of core samples (**Figure 1**). Lithological characteristics are elaborated as follows:

3.1. Detrital Components and Contents

Based on the "Classification and Nomenclature of Sedimentary Rocks (GB/T 17412.2-1998)" standard, detrital components in Benxi Formation sandstones are dominated by quartzose grains (including quartz and chert), followed by lithic fragments and trace feldspar (Mo et al., 2021; Wu et al., 2023). Quartz content ranges from 2.5% to 100%, averaging 77.5%; lithic content from 0% to 97%, averaging 22.3%; and feldspar from 0% to 1.0%, averaging 0.3%. Lithic fragments are predominantly volcanic, succeeded by metamorphic varieties. Lithic constituents mainly include igneous rock fragments and low- to medium-grade metamorphic fragments such as schists, phyllites, slates, and meta-sandstones (**Figure 2**, **Figure 3**).

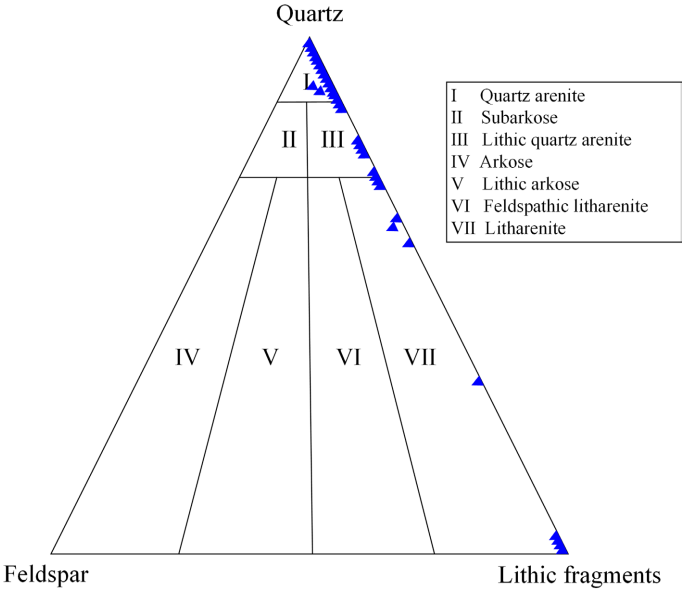

Figure 1. QFL ternary diagram of detrital components in the Yanchuan east block Benxi formation sandstones.

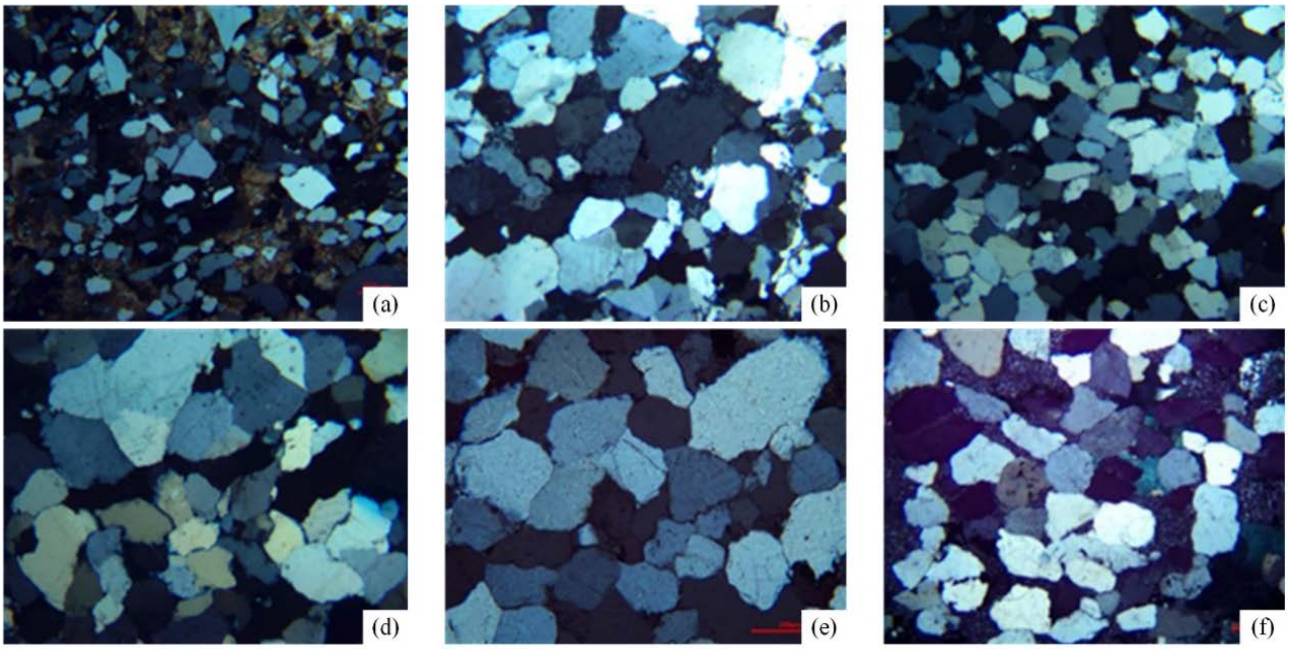

(a) Well Yan 347, Benxi 2, Sample No.: 5-21-35, fine-grained quartz sandstone, early calcite as basal cement. (b) Well Yan 349, Benxi 1, Sample No.: 4-7-118, quartz sandstone, intense compaction with line contacts dominant. (c) Well Yan 387, Benxi 2, Sample No.: 4-14-52, quartz sandstone, intense compaction with line contacts dominant. (d) Well Yan 387, Benxi 2, Sample No.: 4-48-52, quartz sandstone, intense compaction with line and concavo-convex contacts. (e) Well Yan 2064, Sample No.: 5-14-31, Benxi Formation, quartz sandstone, intense compaction. (f) Well An 63, Benxi 2, 2518.60–2518.74 m, lithic quartz sandstone, minor dolomite cement.

Figure 2. Petrographic characteristics of benxi formation sandstones under plane-polarized light in the study area.

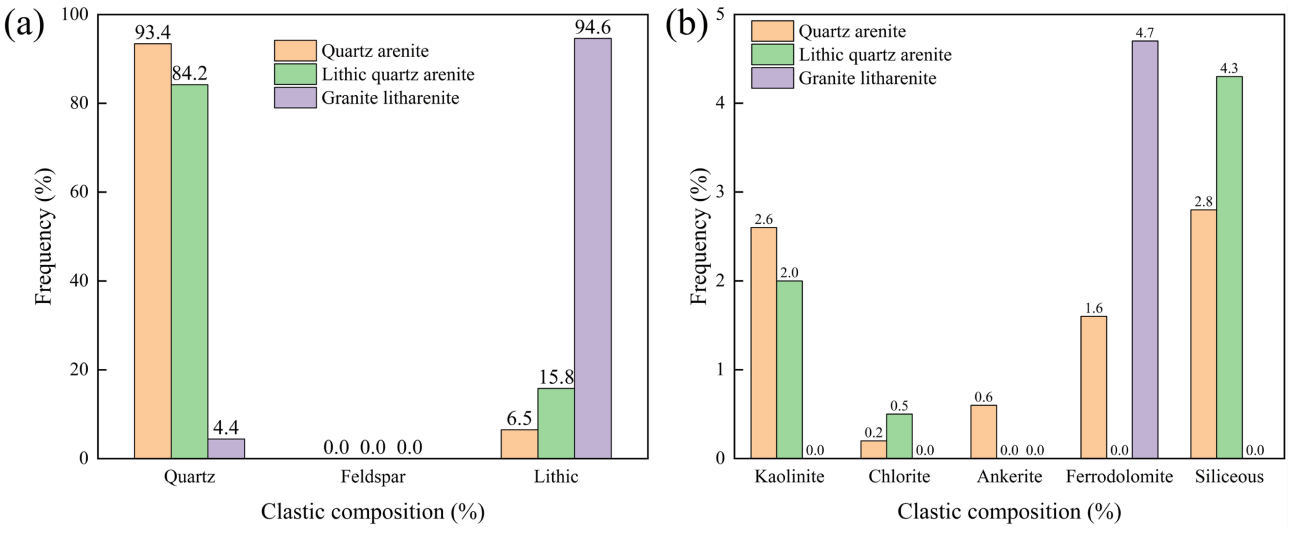

Figure 3. Bar Chart of average component contents in Yanchuan east block Benxi formation sandstones (a: Detrital Components; b: Matrix and Cement Components).

3.2. Matrix and Cement Components and Contents

Authigenic cements in Benxi Formation sandstones primarily comprise carbonates, clay minerals, and siliceous cements (Gao et al., 2022; Ma et al., 2021; Xi et al., 2015a). Carbonate cements include ferroan calcite, ferroan dolomite, and

siderite (Figure 4), with ferroan calcite and ferroan dolomite being relatively abundant. Calcite content ranges from 0% to 35%, averaging 1.69%; dolomite from 0% to 16%, averaging 1.22%. Clay mineral cements are chiefly kaolinite and illite, with minor chlorite (Figure 5). Most kaolinite and chlorite are associated with tuffaceous alteration; kaolinite often exhibits detrital outlines as an alteration product of alkali feldspar and volcanic fragments, while vermiform kaolinite derives from the alteration of feldspar-rich tuff.

4. Reservoir Pore Types and Throat Structure Characteristics

4.1. Reservoir Pore Development Characteristics

The Benxi Formation reservoirs in the Yanchuan East Block primarily exhibit three pore types: residual intergranular pores, secondary dissolution pores, and

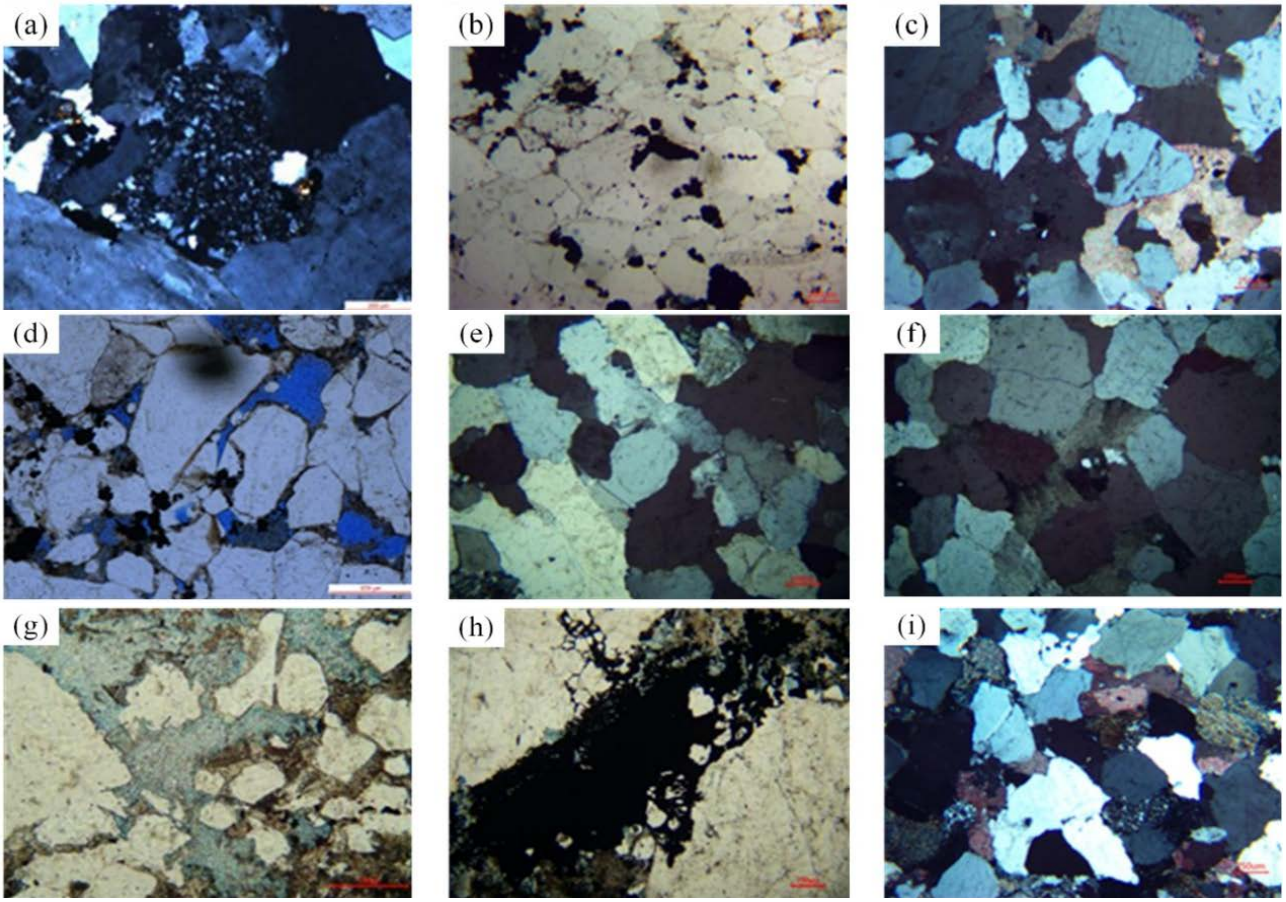

(a) Well Yan 336, Benxi 1, 2580.70 - 2580.91 m, gravelly coarse-grained lithic quartz sandstone, kaolinite filling intergranular pores. (b) Well Yan 336, Benxi 1, Sample No.: 9-44-73, coarse-grained lithic quartz sandstone, pyrite cement filling intergranular pores. (c) Well Yan 272, Benxi 2, Sample No.: 13-63-96, coarse-grained quartz sandstone, calcite as basal cement filling intergranular pores. (d) Well Yan 149, Benxi 1, 2457.80 - 2457.85 m, coarse-grained quartz sandstone, chlorite clay coats developed. (e) Well Yan 2065, Benxi Formation, 2467.01 - 2467.16 m, coarse-grained quartz sandstone, quartz overgrowths developed. (f) Well Yan 2065, Benxi Formation, 2465.64 - 2465.79 m, coarse-grained quartz sandstone, late ferroan dolomite filling intergranular pores. (g) Well Yan 2065, Benxi Formation, 2460.21 - 2460.36 m, early ferroan dolomite as basal cement. (h) Well Yan 2065, Benxi Formation, 2460.21 - 2460.36 m, early pyrite cement and early ferroan dolomite. (i) Well Yan 337, Benxi Formation, Sample No.: 7-50-65, late calcite filling dissolution pores in lithics.

Figure 4. Microscopic characteristics of cements in Benxi formation sandstones in the study area.

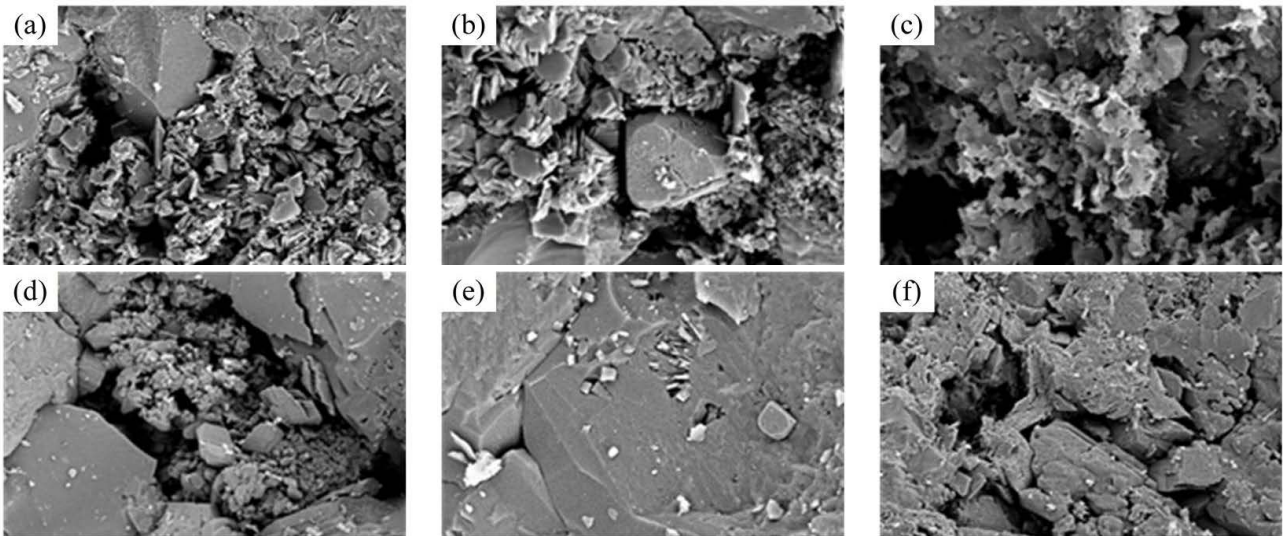

(a) Well Yan 149, Benxi 1, 2455.20 – 2455.25 m; quartz overgrowths and intergranular kaolinite clay matrix. (b) Well Yan 149, Benxi 1, 2457.37 - 2457.66 m; intergranular kaolinite clay filling residual intergranular pores. (c) Well Yan 176, 2777.56 - 2777.68 m; illite-smectite mixed layers, quartz, pyrite filling residual intergranular pores. (d) Well Yan 272, Benxi 2, 2766.5 - 2766.56 m; quartz overgrowths, siderite filling residual intergranular pores. (e) Well Yan 330, Benxi 2, 2699.66 - 2699.86 m; quartz overgrowths, euhedral pyrite crystals. (f) Well Yan 330, Benxi 2, 2699.66 - 2699.86 m; intergranular rhombohedral siderite in residual intergranular pores.

Figure 5. SEM characteristics of cements in Benxi formation sandstones in the study area.

intracrystalline pores. Intergranular pores predominate, accompanied by minor secondary dissolution pores, intracrystalline pores, and microfractures. Secondary dissolution pores mainly include feldspar and volcanic lithic dissolution pores (Chen et al., 2024; Li et al., 2025a; Wang et al., 2023).

① Residual Intergranular Pores: Intense mechanical compaction has affected the Benxi Formation reservoir sandstones in the study area, resulting in widespread residual intergranular pores between quartz grains, albeit with relatively low abundance. These pores are commonly partially filled by clay minerals such as illite and kaolinite, muddy matrix, or authigenic quartz overgrowths (**Figure 6**; **Figure 7**). The pores exhibit irregular morphologies, with diameters typically ranging from 10 to 30 μm.

② Secondary Dissolution Pores: These primarily comprise minor lithic and feldspar dissolution pores within grains, with lithic dissolution pores being dominant and feldspar pores less common. Intragranular dissolution pores occur in isolated or honeycomb patterns, and dissolution may follow cleavage planes within grains (**Figure 6**; **Figure 7**). Pore diameters generally range from 20 to 70 μm, averaging approximately 30 μm.

③ Microfractures: Cast thin-section observations reveal sparse microfracture development. Although fracture density is low, fractures enhance pore connectivity in reservoir sandstones, serving as conduits for hydrocarbon migration. Overall, microfractures in the study area's Benxi Formation are underdeveloped (**Figure 6**; **Figure 7**).

④ Intracrystalline Pores: These pores vary in size and distribution, generally featuring small diameters influenced by crystal size and packing density. They primarily occur within clusters of authigenic clay minerals such as kaolinite, chlorite, and illite. Intracrystalline pore diameters are minute, typically less than 0.01 mm (Figure 6; Figure 7). While intracrystalline pores contribute negligibly to overall storage capacity (comprising < 0.3% of areal porosity), they play a secondary role in enhancing microscale connectivity within clay-rich zones, potentially aiding fluid percolation in otherwise isolated pore networks dominated by intergranular and dissolution pores.

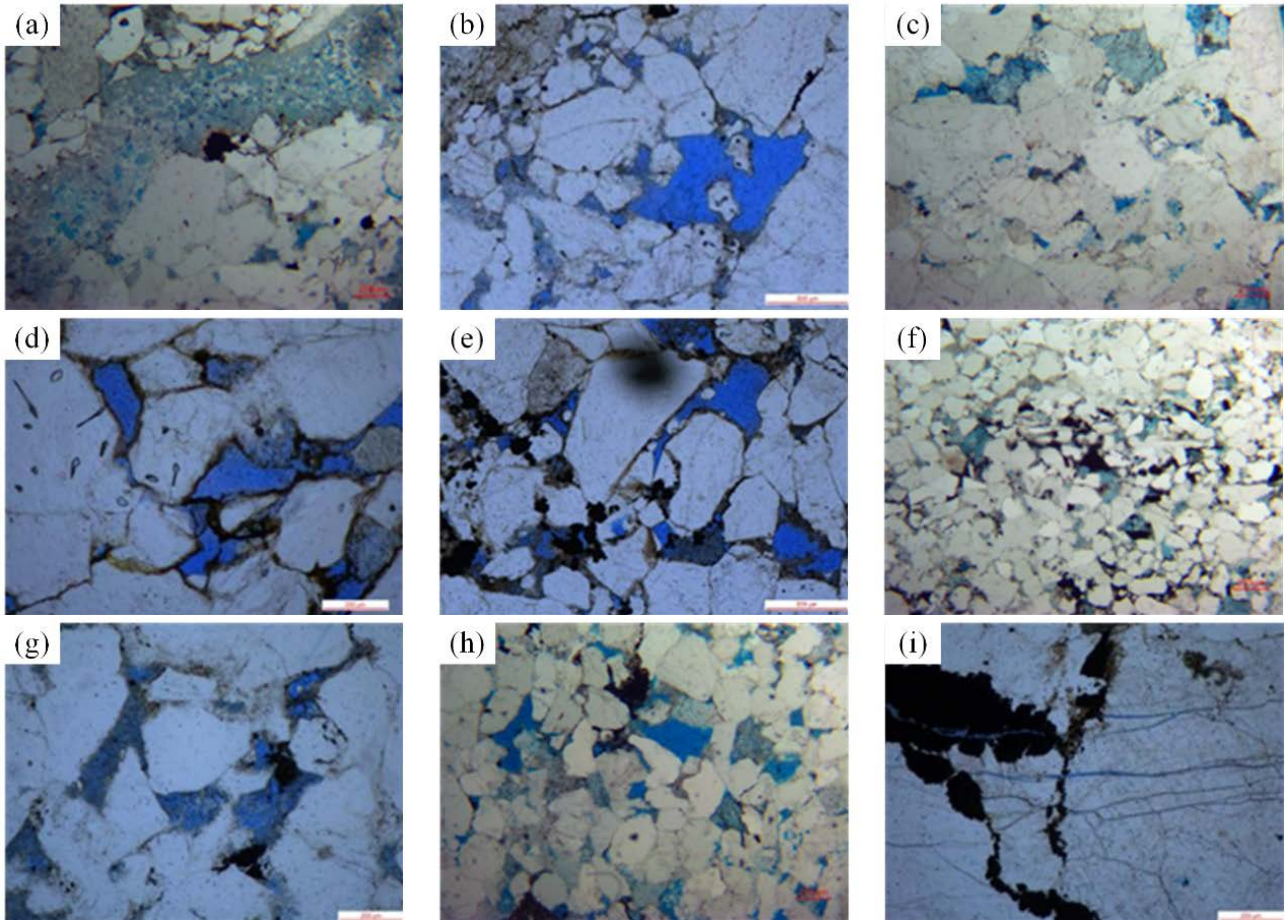

(a) Well Yan 349, Benxi 1, Sample No.: 4-7-118, intragranular dissolution pores in volcanic lithics and minor residual intergranular pores. (b) Well Yan 349, Benxi 1, 2829.49 - 2831.28 m, gravelly coarse- to very coarse-grained lithic quartz sandstone, intergranular pores. (c) Well Yan 349, Benxi 1, Sample No.: 4-14-118, coarse-grained quartz sandstone, intergranular pores and lithic dissolution pores. (d) Well Yan 349, Benxi 1, 2831.28 - 2833.09 m, medium- to coarse-grained quartz sandstone, intergranular pores. (e) Well Yan 149, Benxi 1, 2457.80 - 2457.85 m, coarse-grained quartz sandstone, intergranular pores. (f) Well Yan 272, Benxi 1, Sample No.: 13-29-96, lithic quartz sandstone, lithic dissolution pores and minor residual intergranular pores. (g) Well Yan 272, Benxi 2, 2767.85 - 2767.91 m, fine- to medium-grained quartz sandstone, volcanic lithic dissolution pores. (h) Well Yan 304, Benxi 2, lithic quartz sandstone, intergranular pores and lithic dissolution pores. (i) Well Yan 336, Benxi 1, 2580.70 - 2580.91 m, gravelly very coarse- to coarse-grained lithic quartz sandstone, minor microfractures.

Figure 6. Cast thin-section petrographic characteristics of pore types in Benxi formation sandstones in the study area.

Statistical analysis indicates that the areal porosity of Benxi Formation sandstones ranges from 0.3% to 5.30%, averaging 3.6%. Pore types are dominated by

volcanic lithic dissolution pores (0.2% - 4.8%, averaging 2.8%) and residual intergranular pores (0.3% - 4.3%, averaging 0.55%), with minor microfractures and intracrystalline micropores. The average areal porosity of microfractures and intracrystalline pores is approximately 0.3%.

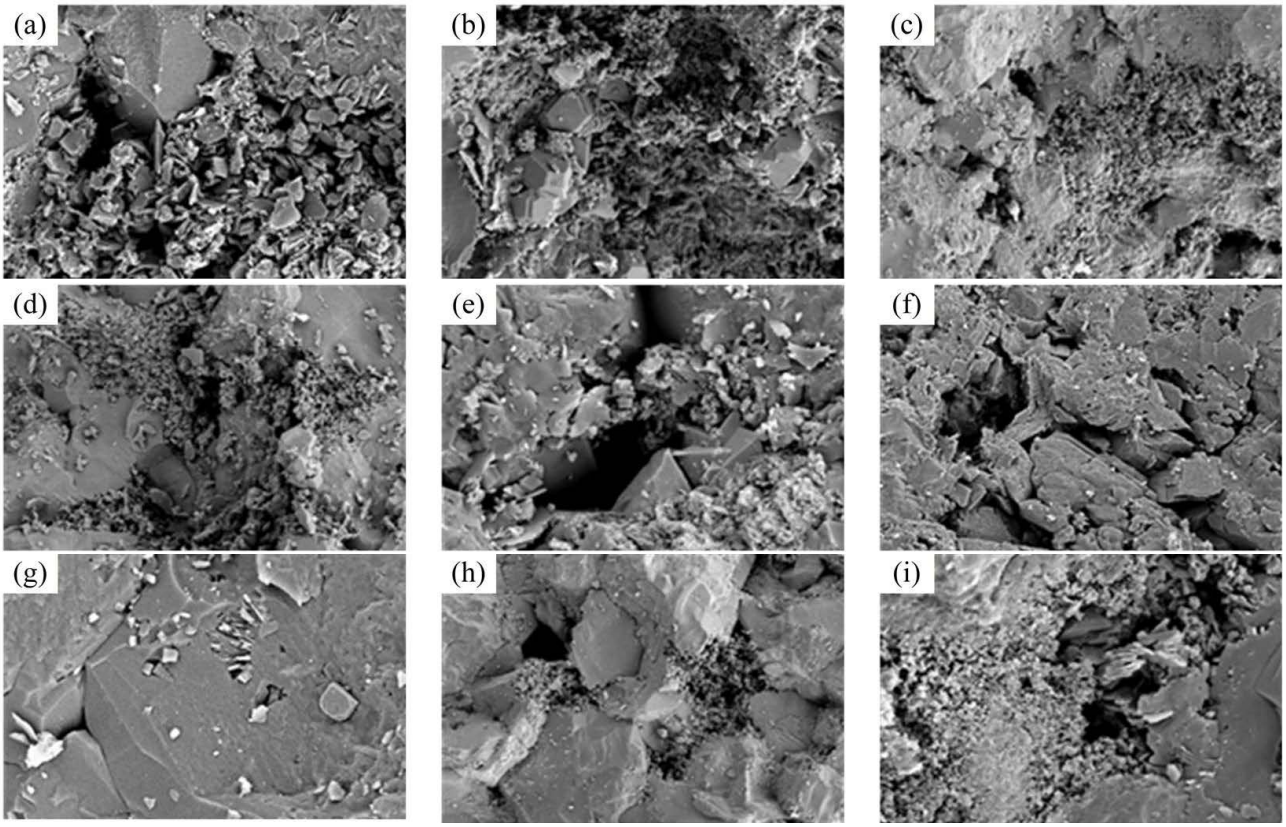

(a) Well Yan 149, Benxi 1, 2455.20 - 2455.25 m, residual intergranular pores. (b) Well Yan 149, Benxi 1, 2455.20 - 2455.25 m, intragranular dissolution pores in volcanic lithics. (c) Well Yan 149, Benxi 1, 2457.37 - 2457.66 m, residual intergranular pores and volcanic lithic dissolution pores. (d) Well Yan 176, Benxi 2, 2777.56 - 2777.68 m, residual intergranular pores and volcanic lithic dissolution pores. (e) Well Yan 272, Benxi 2, 2766.50 - 2766.56 m, residual intergranular pores. (f) Well Yan 330, Benxi 2, 2699.66 - 2699.86 m, intragranular lithic dissolution pores and minor intracrystalline pores. (g) Well Yan 330, Benxi 2, 2699.66 - 2699.86 m, minor intracrystalline micropores. (h) Well Yan 336, Benxi 1, 2578.52 - 2578.67 m, residual intergranular pores and volcanic lithic dissolution pores. (i) Well Yan 349, Benxi 1, 2829.49 - 2831.28 m, intragranular dissolution pores in volcanic lithics.

Figure 7. SEM characteristics of pore types in Benxi formation sandstones in the study area.

4.2. Throat Structure Characteristics

High-pressure mercury intrusion commonly measures pore structure parameters, including those for throat size (displacement pressure and maximum throat radius; median pressure and median radius; average throat volume ratio), distribution (sorting coefficient, skewness coefficient, kurtosis), and connectivity (maximum mercury saturation and mercury expulsion efficiency) (Zhang et al., 2024, 2020; Zhu et al., 2024).

For Benxi Formation sandstones, displacement pressure ranges from 0.01 to 1.54 MPa, averaging 0.71 MPa; median pressure from 1.98 to 69.46 MPa, averaging 20.29 MPa; and median radius from 0.10 to 0.37 μm, averaging 0.14 μm, indi-

cating overall small pores but relatively larger throats. The sorting coefficient ranges from 0.05 to 4.43, averaging 2.43 (poor sorting); skewness from 0.11 to 0.77, averaging 0.31; and maximum mercury saturation from 62.55% to 96.76%, averaging 79.21%, signifying good connectivity. Overall, Benxi Formation sandstone throats are slightly small, poorly sorted, but well-connected (Table 1).

Table 1. Statistical table of high-pressure mercury intrusion parameters for Benxi formation sandstones in the Yanchuan east area, Yanan gas field.

Parameter		Petrophysical Properties		Throat Size			Throat Sorting Characteristics			Throat Connectivity	
Stratigraphic horizon	Number of samples	Porosity (%)	Permeability (mD)	Displacement pressure (MPa)	Median pressure (MPa)	Median radius (μm)	Sorting coefficient of pore-throat	Coefficient of variation	Skewness coefficient	Maximum mercury saturation (%)	Withdrawal efficiency (%)
Benxi Formation	Minimum	2.10	0.023	0.01	1.98	0.01	0.05	0.11	-0.22	62.55	18.25
28	Maximum	7.24	2.409	1.54	69.46	0.37	4.43	0.77	2.23	96.76	41.23
	Average	4.28	0.267	0.71	20.29	0.14	2.43	0.31	1.31	79.21	30.36

Following the "Evaluation Methods for Oil and Gas Reservoirs (SY/T 6285–2011)" classification for clastic reservoir pore structures, analysis of mercury intrusion parameters, combined with petrophysical properties and capillary pressure curve shapes, delineates four throat structure types for Upper Paleozoic sandstones in the Yanchuan East Block (Figure 8).

Type I (Low Displacement Pressure-Coarse Throat Type)

Capillary pressure curves for this type exhibit displacement pressures of 0.01 – 1.74 MPa (average 0.52 MPa), median pressures of 0.33 – 21.21 MPa (average 3.08 MPa), and average throat radii of 0.09 - 11.26 μm (average 1.73 μm). Skewness ranges from −0.22 to 2.49 (average 0.94, coarse-skewed); sorting coefficient from 0.14 to 0.33 (average 0.18); and maximum mercury saturation from 83.65% to 99.04% (average 92.22%). Curves trend toward the lower left with broad horizontal platforms (Figure 8(a)). Reservoirs of this type feature coarse throats with variable pore sorting. Porosity ranges from 2.10% to 9.00% (average 6.33%), and permeability from 0.057 to 4.723 mD (geometric mean 0.836 mD). These occur in composite-pore quartz sandstones dominated by residual intergranular pores with intense dissolution, where large and small pores coexist, throats are coarse, and connectivity is excellent, representing high-quality reservoirs. This type is common in the Benxi Formation.

Type II (Medium Displacement Pressure-Fine Throat Type)

Displacement pressures range from 0.01 to 6.32 MPa (average 0.60 MPa), median

pressures from 0.27 to 36.15 MPa (average 4.66 MPa), and average throat radii from 0.02 to 6.66 μm (average 1.29 μm). Skewness ranges from −0.28 to 2.11 (predominantly coarse-skewed); sorting coefficient from 0.11 to 1.04 (average 0.30); and maximum mercury saturation from 72.90% to 95.80% (average 83.29%). Curves slightly trend lower left, with or without broad platforms (Figure 8(b)). Reservoirs feature fine throats with variable pore sorting. Porosity ranges from 1.82% to 11.57% (average 6.27%), but permeability is lower, from 0.016 to 4.143 mD (geometric mean 0.688 mD). These occur in quartz, lithic quartz, or lithic sandstones with dominant intergranular–lithic dissolution or intergranular–intracrystalline pore assemblages, intense dissolution, and moderate connectivity, representing good reservoirs. This type is widespread in the Benxi Formation.

Type III (Medium Displacement Pressure-Microfine Throat Type)

Displacement pressures range from 0.02 to 1.82 MPa (average 0.70 MPa), median pressures from 3.26 to 88.72 MPa (average 43.96 MPa), and average throat radii from 0.14 to 0.62 μm (average 0.34 μm). Skewness ranges from 0.90 to 2.69 (fine- to

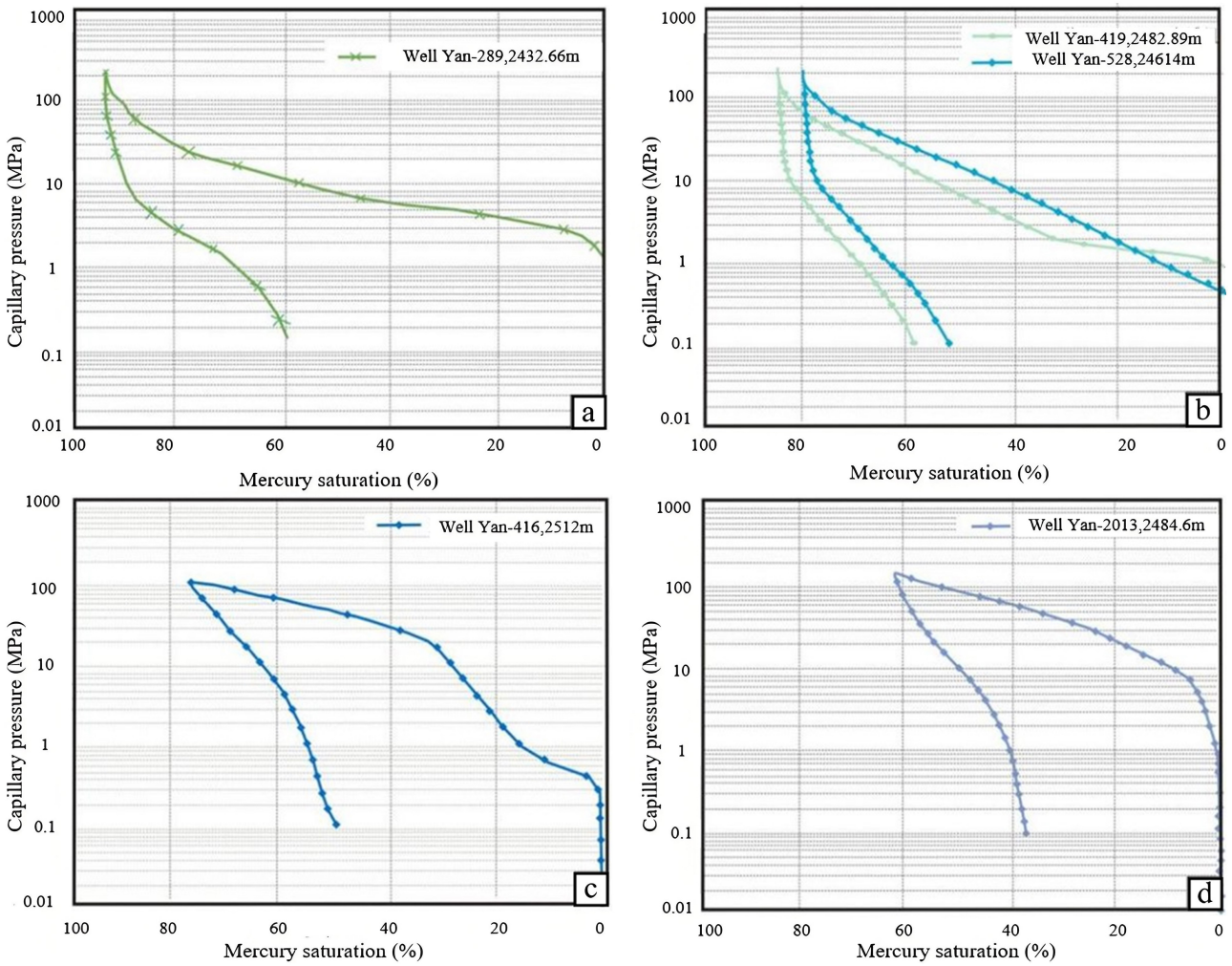

(a) Type I Reservoir; (b) Type II Reservoir; (c) Type III Reservoir; (d) Type IV Reservoir.

Figure 8. Typical mercury intrusion capillary pressure curves for Benxi formation reservoir sandstones.

coarse-skewed); sorting coefficient from 0.12 to 0.51 (average 0.27); and maximum mercury saturation from 63.40% to 91.26% (average 78.22%). Curves form steep slopes without platforms (Figure 8(c)). Porosity ranges from 0.80% to 1.63% (average 1.07%), and permeability from 0.012 to 1.681 mD (geometric mean 0.257 mD). These occur in lithic quartz or lithic sandstones dominated by intracrystalline or intragranular dissolution pores, with small pores, moderate sorting, and connectivity.

Type IV (High Displacement Pressure–Microfine Throat Type)

Displacement pressures range from 0.13 to 7.61 MPa (average 1.53 MPa), with median pressures exceeding 50 MPa; average throat radii from 0.02 to 0.20 μm (average 0.13 μm); skewness from -2.08 to 2.23 (predominantly fine-skewed); and sorting coefficient from 0.08 to 0.80 (average 0.32). Curves form convex upper-right steep slopes (Figure 8(d)). Porosity ranges from 1.79% to 5.30% (average 3.19%), and permeability from 0.003 to 0.131 mD (geometric mean 0.024 mD). Reservoirs feature micropores or intracrystalline pores, small throats, and poor connectivity, rendering them ineffective.

5. Diagenetic Processes and Reservoir Evolution Analysis

5.1. Reservoir Petrophysical Characteristics

Core petrophysical analysis in the study area reveals that Benxi Formation reservoir porosity ranges from 0.17% to 9.07% (average 4.74%, median 3.83%). Most values (91.32%) fall between 2% and 7%, with 3.72% exceeding 7% and 4.96% below 2%. Permeability ranges from 0.01 to 6.05 mD (geometric mean 0.91 mD, median 0.06 mD), with 75.42% between 0.05 and 0.15 mD, 19.49% above 0.15 mD, and 5.08% below 0.05 mD (Figure 9).

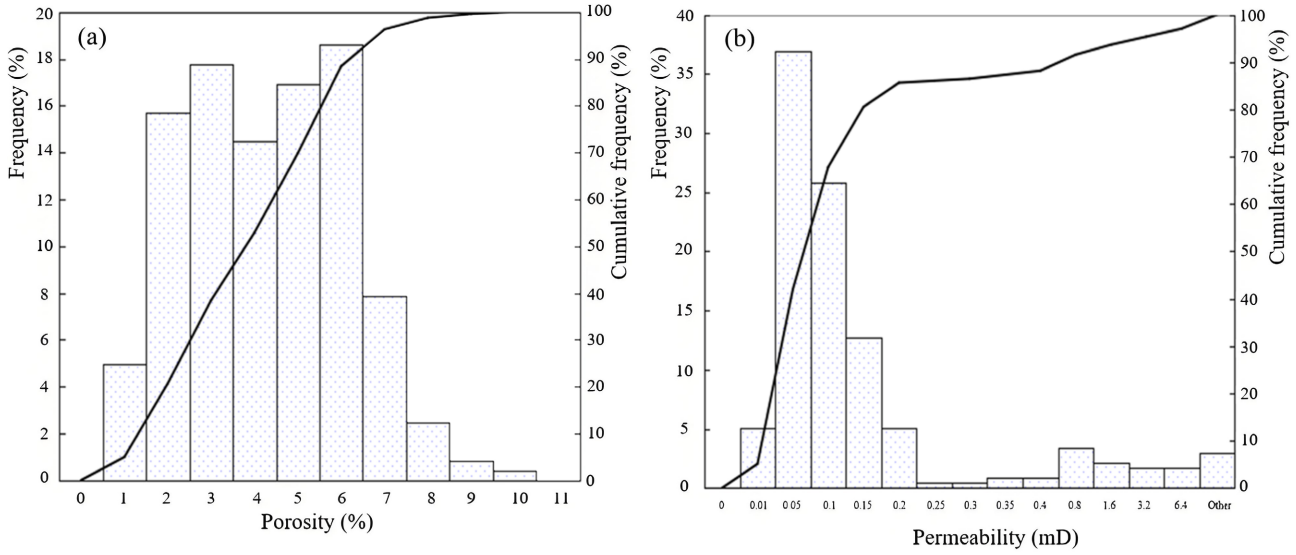

Figure 9. Histogram of atmospheric core petrophysical properties for Benxi formation in the Yanchuan east block.

5.2. Reservoir Classification Evaluation

Per the "Norms for Estimation of Oil and Gas Resources (DZ/T 0217–2020)"

petrophysical classification (Table 2), reservoirs are categorized into six classes. Core data from the Yanchuan East Block show Benxi Formation overburden porosity of 3.0% - 14.9% (mean 5.4%, median 5.3%) and overburden permeability of 0.011 - 4.328 mD (median 0.078 mD). Thus, the block's Benxi Formation sandstones classify as ultra-low porosity and tight reservoirs.

Table 2. Porosity and permeability classification for reservoirs (DZ/T 0217–2020).

Classification	Porosity (%)		Permeability (mD)
	Clastic rock porosity (%)	Non-clastic matrix porosity (%)	Reservoir air permeability
Ultra-High	≥30	≥15	≥500
High	≥25 - <30	≥10 - <15	≥100 - <500
Medium	≥15 - <25	≥5 - <10	≥10 - <100
Low	≥10 - <15	≥2 - <5	≥1.0 - <10
Ultra-Low	<10	<2	≥0.1 - <1.0
Tight			<0.1

5.3. Diagenetic Characteristics

Thin-section, cast thin-section, SEM, XRD, and fluorescence analyses delineate diagenetic types and sequences for study area reservoir sandstones. Benxi Formation diagenesis divides into eodiagenesis and mesodiagenesis, with principal processes: mechanical compaction, cementation, and dissolution.

5.3.1 Typical Diagenetic Features

1) Mechanical Compaction

Compaction involves dewatering, porosity reduction, and volume decrease under overburden or tectonic stress post-deposition. Rigid grains (quartz, feldspar) undergo sliding, rotation, displacement, deformation, or fracturing, rearranging particles and altering structures; minor matrix fills pores. Post-intense compaction, Benxi Formation clastics are grain-supported, with rigid fragments showing line or concavo-convex contacts and severe primary intergranular pore destruction (Figure 10(a)-(b)). High plastic grain content (mica, mud clasts) leads to deformation or pseudomatrix formation, destroying primary pores (Figure 10(c), d). Sensitivity increases above 12% matrix, causing rapid compaction and pore loss. Plastic lithics like mica deform into pseudomatrix, reducing pores without cement (Figure 10(e)). Deeper burial transitions to pressure solution: quartz resists most, feldspar intermediately, lithics least. Quartz pressure solution forms overgrowths, consuming intergranular pores and degrading properties via enhanced contacts (Figure 10(f)).

2) Dissolution

Dissolution involves selective mineral removal during diagenesis to achieve physicochemical equilibrium, driven by environmental changes. Early dissolution relates to meteoric leaching; later to organic acids from kerogen maturation below

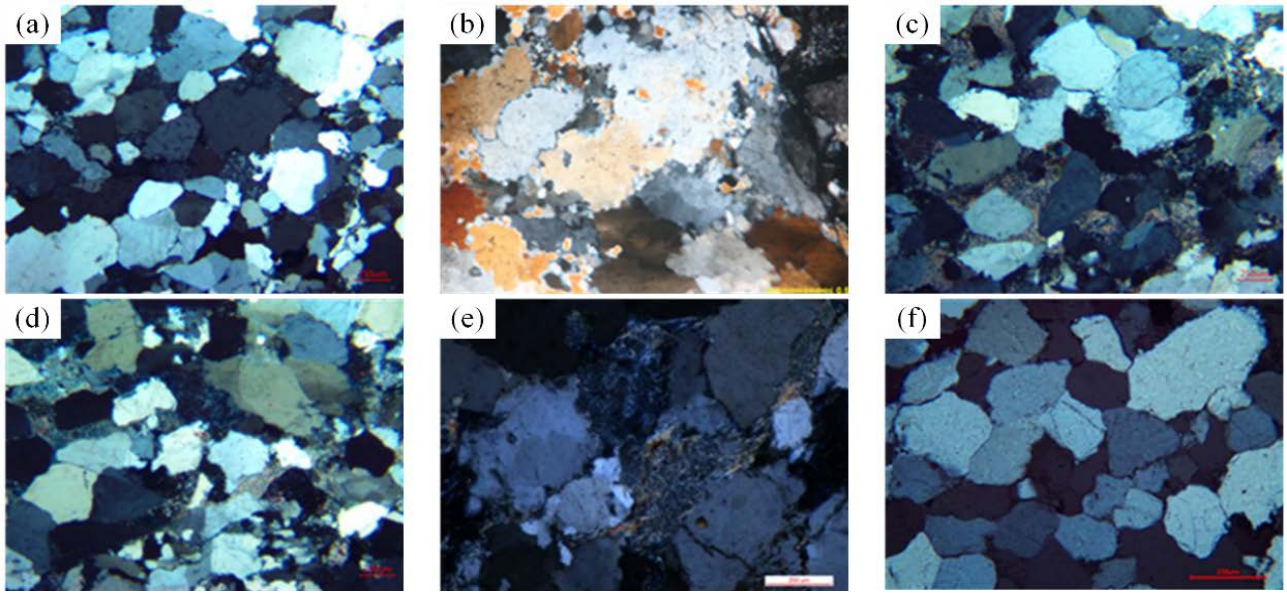

(a) Well Yan 349, Benxi Formation, Sample No.: 4-7-118, quartz sandstone, line grain contacts, minor volcanic lithic deformation. (b) Well Yan 1827, Benxi Formation, 2511.73 - 2512 m, lithic sandstone, intense granitic lithic compaction with concavo-convex contacts. (c) Well Yan 337, Benxi Formation, Sample No.: 7-31-65, lithic quartz sandstone, intense plastic deformation of volcanic lithics. (d) Well Yan 337, Benxi Formation, Sample No.: 7-42-65, lithic quartz sandstone, intense plastic deformation of volcanic lithics. (e) Well Yan 337, Benxi Formation, Sample No.: 7-64-52, lithic quartz sandstone, intense volcanic lithic deformation into pseudomatrix. (f) Well Yan 2064, Sample No.: 5-14-31, Benxi Formation, quartz sandstone, intense compaction.

Figure 10. Characteristics of mechanical compaction in Benxi formation reservoir sandstones in the study area.

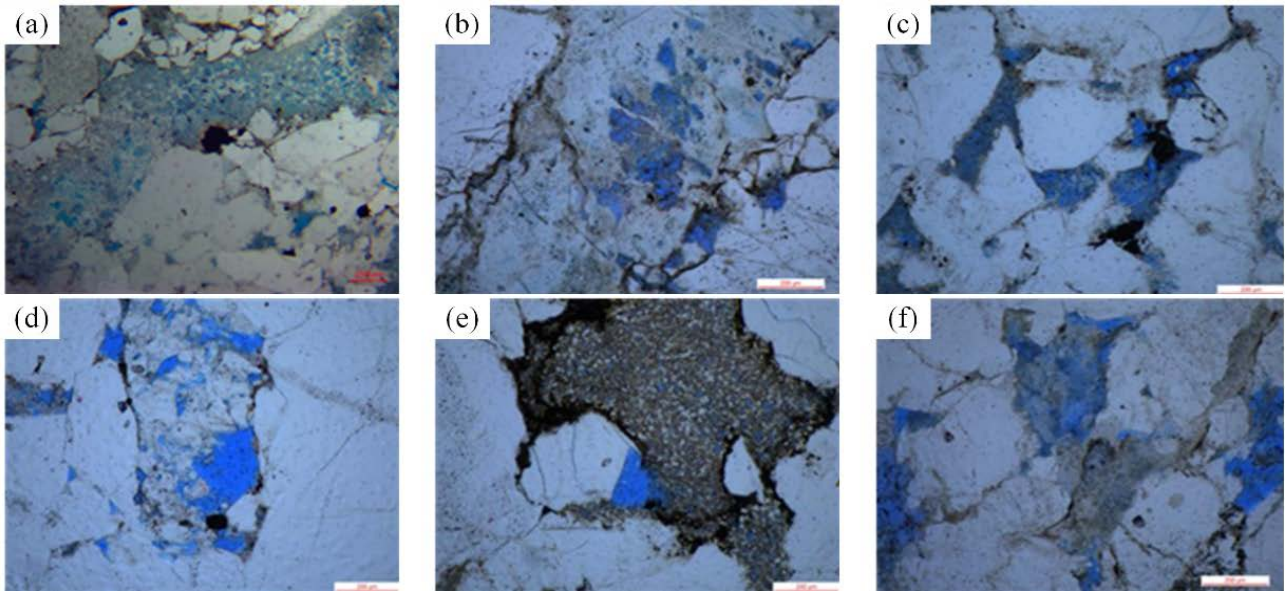

(a) Well Yan 349, Benxi 1, Sample No.: 4-7-118, selective dissolution of volcanic lithics. (b) Well Yan 349, 2829.49 - 2831.28 m, gravelly coarse- to very coarse-grained lithic quartz sandstone, lithic dissolution. (c) Well Yan 272, 2767.85 - 2767.91 m, fine- to medium-grained quartz sandstone, intragranular volcanic lithic dissolution pores. (d) Well Yan 330, 2694.65 - 2694.85 m, gravelly medium- to coarse-grained quartz sandstone, lithic dissolution pores. (e) Well Yan 336, 2580.70 – 2580.91 m, lithic quartz sandstone, intracrystalline pores from kaolinite replacing lithics. (f) Well Yan 337, 2740.11 - 2740.21 m, medium- to coarse-grained lithic sandstone, volcanic lithic dissolution pores.

Figure 11. Characteristics of dissolution in Benxi formation reservoir sandstones in the study area.

oil window depths. Observations show pervasive but moderate dissolution in the study area, targeting unstable lithics, carbonates, and cements, forming secondary pores. Selective dissolution causes uneven pore distribution (Figure 11). In Benxi Formation reservoirs, feldspar-rich volcanic lithics undergo selective dissolution, forming secondary pores and enhancing properties. Minor lithic dissolution occurs in quartz sandstones; more in lithic quartz sandstones. This yields intergranular + intragranular pore assemblages (Figure 11).

3) Cementation

Cementation precipitates minerals from pore fluids, binding sediments and reducing porosity/permeability. In the study area, it includes siliceous, carbonate, clay mineral, and pyrite types. Growth modes vary: overgrowths (e.g., silica on quartz), edge cements (clay rims), or infills (carbonates, zeolites).

① Siliceous Cementation

Silica supersaturation in pore fluids precipitates as quartz overgrowths or authigenic crystals on grain surfaces, or fine infills. Overgrowths show multiphase growth, thick and ubiquitous (Figure 12(a)-(c)), filling pores and clogging throats, impairing permeability (Figure 12(d)). Authigenic quartz, post-compaction, derives from feldspar/lithic dissolution or pressure solution, occurring as singles or aggregates (Figure 12(e)-(f)). It reduces primary pores and influences secondary ones. Siliceous cements average 1% - 5% in Benxi Formation reservoirs.

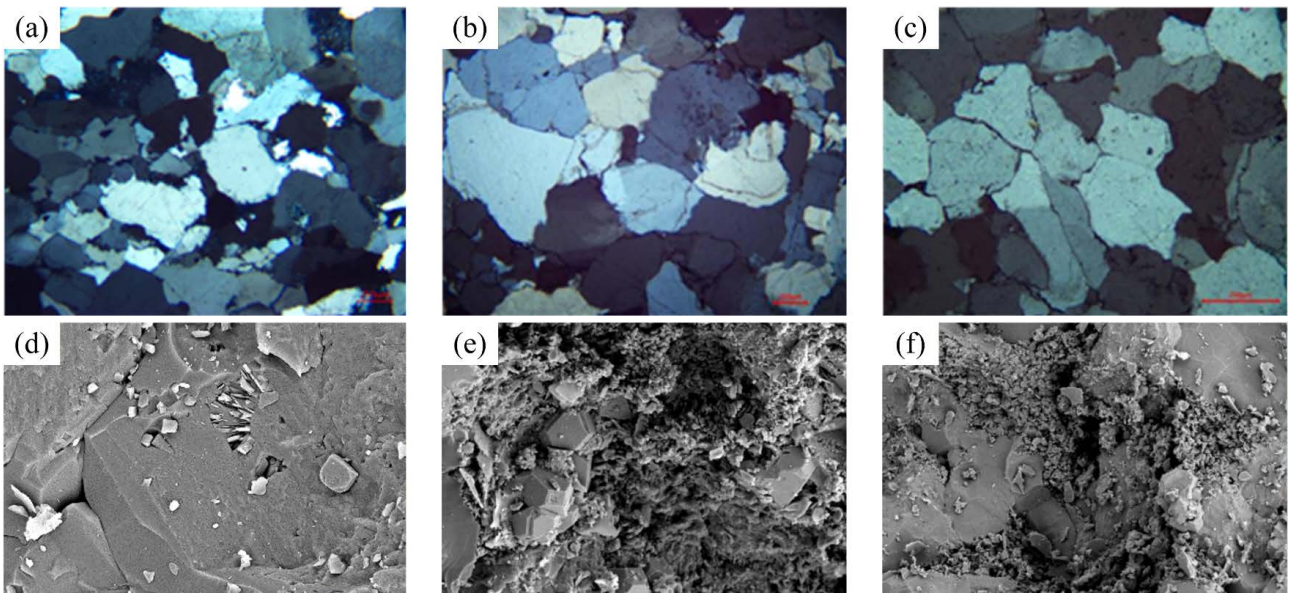

(a) Well Yan 349, Benxi 1, Sample No.: 4-14-118, quartz overgrowths. (b) Well Yan 2064, Benxi Formation, Sample No.: 5-29-31, widespread quartz overgrowths. (c) Well Yan 2064, Benxi Formation, 2455.16 - 2455.41 m, widespread quartz overgrowths. (d) Well Yan 330, Benxi 2, 2699.66 - 2699.86 m, quartz overgrowths and euhedral pyrite. (e) Well Yan 149, Benxi 1, 2455.20–2455.25 m, intragranular volcanic lithic dissolution pores and authigenic quartz. (f) Well Yan 176, Benxi 2, 2777.56 - 2777.68 m, volcanic lithic dissolution pores and authigenic quartz.

Figure 12. Characteristics of siliceous cementation in Benxi formation reservoir sandstones in the study area.

② Carbonate Cementation

Carbonates precipitate throughout diagenesis, varying in crystallography and

composition due to fluid-rock interactions, pH, and redox conditions. Predominant calcite forms three phases.

I. Early Calcite Cementation

Micritic to microcrystalline carbonates precipitate from near-surface pore waters under low temperature/pressure when CaCO3 supersaturates in alkaline conditions. They form basal cements filling intergranular spaces, comprising calcite (occasional ferroan dolomite), 5% - 10% abundant, yielding calcareous sandstones. Grains float in cement with high intergranular volume, pre-compaction (Figure 13).

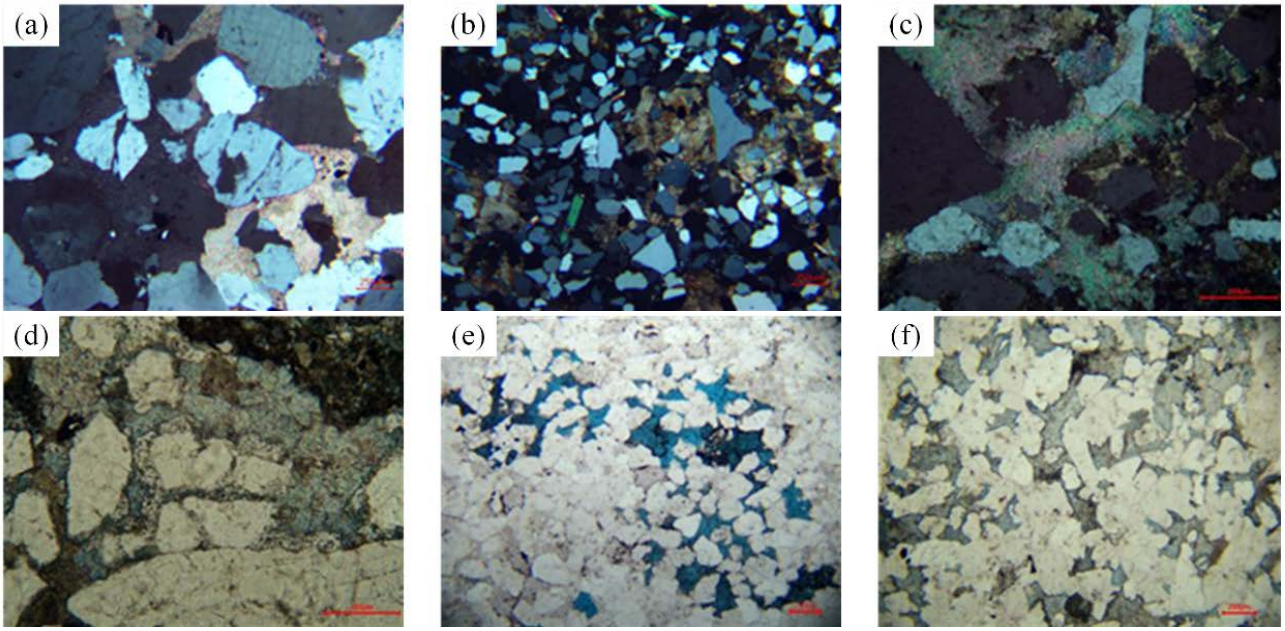

(a) Well Yan 272, Benxi 2, Sample No.: 13-63-96, early calcite as basal cement filling intergranular pores. (b) Well Yan 347, Benxi 2, Sample No.: 5-21-35, early calcite as basal cement. (c) Well Yan 2065, Benxi Formation, 2460.21 - 2460.36 m, early ferroan dolomite basal cement replacing quartz edges. (d) Well Yan 2065, Benxi Formation, 2460.51 - 2460.72 m, early ferroan dolomite basal cement replacing quartz edges. (e) Well An 63, Benxi Formation, 2520.39 - 2520.61 m, early ferroan dolomite as nodular basal cement. (f) Well Yan 2065, Benxi Formation, 2459.76 - 2459.93 m, early ferroan dolomite basal cement replacing quartz edges.

Figure 13. Petrographic characteristics of early carbonate cements in Benxi formation in the study area.

II. Middle Carbonate Cementation

In late eodiagenesis, increased temperature/pressure compacts grains, reducing pore space to residual intergranular pores under weakly alkaline fluids. Supersaturation precipitates pore-filling cements (Figure 14(a)-(b)). Dispersed pore cements comprise ferroan calcite, clean and coarse-crystalline, 2% – 10%, forming calcic sandstones.

III. Late Ferroan Calcite Cementation

In mesodiagenesis, deep burial, high temperature/pressure, and reducing conditions enrich pore fluids in Fe^{2+}/Mg^{2+} from clay alteration. Reduced CO_2 partial pressure incorporates ions into calcite/dolomite lattices. Late cements infill intergranular and dissolution pores as dispersed or granular ferroan calcite/dolomite,

clean and fine-crystalline, 2% - 5% (Figure 14(c)-(f)). They postdate and replace earlier cements/quartz, marking the latest phase and contributing to late porosity reduction.

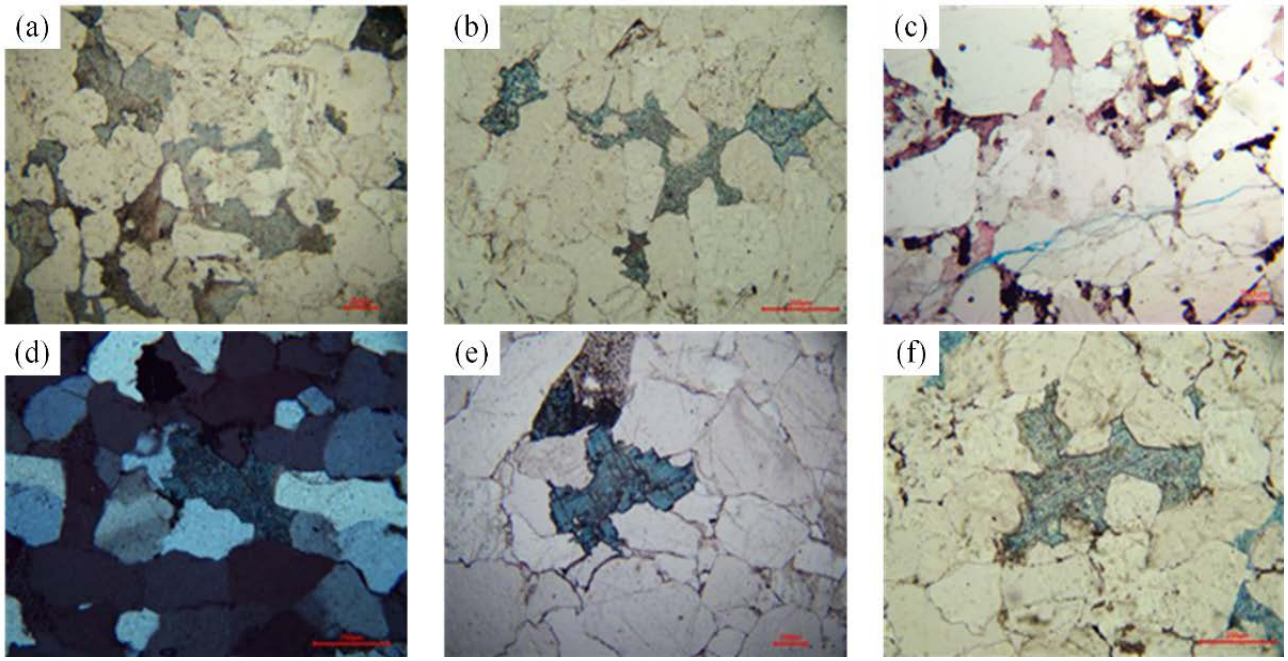

(a) Well Yan 2065, Benxi Formation, 2467.01 - 2467.16 m, middle ferroan dolomite as pore-filling cement in intergranular pores. (b) Well Yan 2065, Benxi Formation, 2455.16 - 2455.41 m, middle ferroan dolomite as pore-filling cement in intergranular pores. (c) Well Yan 272, Benxi 2, Sample No.: 13-63-96, late calcite filling residual intergranular and intragranular dissolution pores. (d) Well Yan 2064, Benxi Formation, Sample No.: 5-14-31, late ferroan dolomite as pore-filling cement. (e) Well Yan 2064, Benxi Formation, Sample No.: 5-29-31, late ferroan dolomite filling residual intergranular and dissolution pores. (f) Well Yan 2065, Benxi Formation, 2454.71 - 2454.92 m, late ferroan dolomite filling residual intergranular and dissolution pores.

Figure 14. Petrographic characteristics of middle and late carbonate cements in Benxi formation in the study area.

③ Authigenic Clay Mineral Cementation

Cast thin-sections, SEM, and XRD identify chlorite, kaolinite, illite-smectite mixed layers, and illite. Illite forms irregular, curved, or filamentous coatings on grains or fills fractures, with bridging in residual intergranular spaces. Chlorite occurs as early grain-coating films or late pore fills, with films predominant (Figure 11(c)). Minor platy or honeycomb illite-smectite fills intergranular pores or coexists with authigenic minerals, forming during deep burial. Kaolinite forms hexagonal platelets or aggregates in volcanic lithic pores, often with authigenic quartz (Figure 12(e)-(f)).

④ Pyrite Cementation

Minor pyrite forms early basal cements or late nodular/granular infills in intergranular pores, indicating enclosed reducing conditions during burial diagenesis (Figure 15).

Quantitative estimation of porosity evolution, based on integrated thin-section porosity measurements, compaction modeling, and cement volume calculations, indicates that mechanical compaction accounts for approximately 40% - 50% of

primary porosity loss (reducing initial −25% - 30% depositional porosity to −12% - 15%), while multiphase cementation (siliceous, carbonate, and clay) contributes 30% - 40% additional loss (further reducing to −5% - 8%). Conversely, selective dissolution during mesodiagenesis recovers 20% - 30% of porosity through secondary pore creation, partially offsetting densification and enabling localized reservoir enhancement.

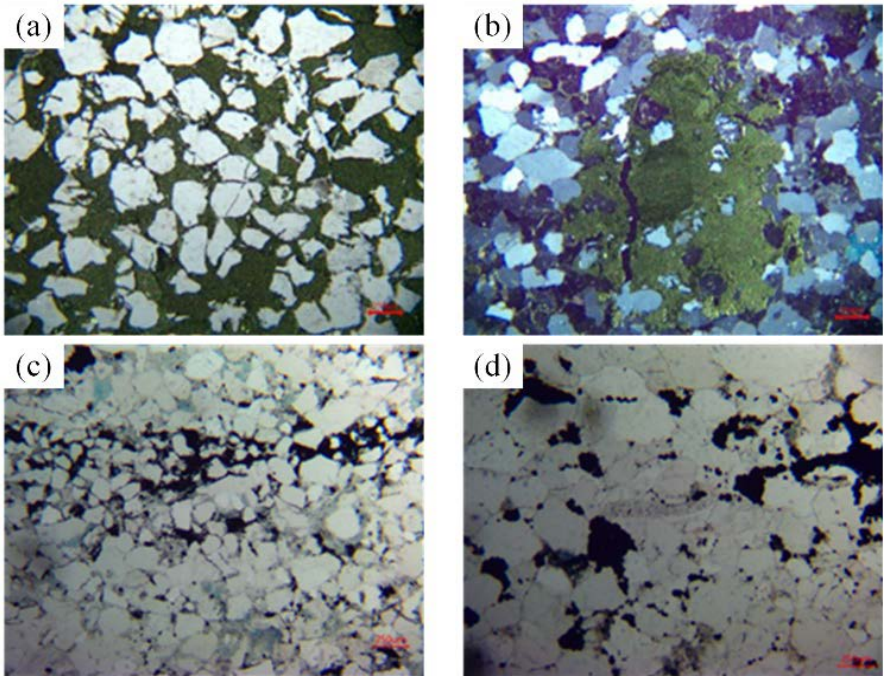

(a) Well An 63, Benxi Formation, 2518.05 - 2518.20 m, early pyrite as basal cement. (b) Well An 63, Benxi Formation, 2520.98 - 2521.10 m, early pyrite as nodular. (c) Well Yan 272, Benxi 2, Sample No.: 13-29-96, early pyrite in banded distribution. (d) Well Yan 336, Benxi 1, Sample No.: 9-44-73, pyrite filling intergranular spaces.

Figure 15. Petrographic characteristics of pyrite cements in Benxi formation reservoirs in the study area.

5.3.2. Diagenetic Stage Division

Based on burial depth, rock fabric, pore types/assemblages, authigenic mineral sequences, clay assemblages, paleotemperature, organic maturity (vitrinite reflectance Ro, Tmax), hydrocarbon charge timing, diagnostic minerals in acidic/alkaline settings, and mineral-pore relations—integrated with regional geology—diagenetic stages are delineated using the following thresholds specific to the Ordos Basin context: eodiagenesis (burial depth < 2 km, temperature < 70˚C, Ro < 0.5%); mesodiagenesis A (burial 2 - 3.5 km, 70˚C - 120˚C, Ro 0.5% - 1.3%); and mesodiagenesis B (>3.5 km, >120˚C, Ro >1.3%).

1) Eodiagenesis

Shallow burial yields weak compaction, point-line grain contacts, and abundant primary pores (>25% porosity). Well-sorted barrier island sands have good pore-throat properties. Under early fluids, early calcite supersaturates in alkaline conditions as basal cement. Chlorite coats grains constructively, preserving pores. Ze-

olite cements precipitate as interlocking infills. Early compaction destroys −50% primary porosity.

In late eodiagenesis B, deeper burial intensifies compaction and cementation (quartz overgrowths, authigenic kaolinite). Contacts remain point-line; cements shift to pore-filling. Combined effects consolidate sandstones, reducing porosity to −15%.

2) Mesodiagenesis A

Early mesodiagenesis A sees low-maturity kerogen releasing organic acids, shifting to weakly acidic conditions. Selective dissolution of feldspars, volcanic lithics, and zeolites generates secondary pores, improving properties. Silica enters fluids, sourcing later quartz cements that overgrow grains, filling pores and clogging throats. This stage aligns with initial hydrocarbon charging in the Early Jurassic, where dissolution-enhanced pores begin trapping early-migrating gases from underlying coal measures.

3) Mesodiagenesis B

Intensified dissolution consumes acids, shifting to weakly alkaline conditions. Cementation strengthens with authigenic quartz and minor ferroan dolomite as pore-fills, further degrading properties. Late hydrocarbon charging in the Middle Jurassic to Early Cretaceous coincides with this stage, leveraging residual connected pore networks (from prior dissolution) for efficient gas accumulation and sealing against overpressured cements.

6. Conclusion

Benxi Formation sandstones in the Yanchuan East Block comprise mainly quartz sandstones, lithic quartz sandstones, and lithic sandstones, with high quartz content, widespread volcanic lithics, moderate sorting, and complex cements. Pores are dominated by residual intergranular and secondary dissolution types, with minor intracrystalline pores and microfractures; overall low porosity and permeability characterize ultra-low porosity, ultra-low permeability tight sandstones. Mercury intrusion reveals microfine throats classifiable into four types, with Types I and II exhibiting good connectivity as primary high-quality reservoirs, while Types III and IV feature small pores and poor connectivity, rendering them low-efficiency or ineffective and dictating heterogeneous spatial distribution and hydrocarbon enrichment. Diagenesis profoundly controls evolution: early intense compaction and multiphase cementation drive densification, whereas middle-late selective dissolution locally ameliorates structures, yielding "pervasively densified yet locally effective" reservoirs. These insights deepen understanding of Benxi Formation reservoirs in the Yanchuan East Block, furnishing key geological bases for favorable reservoir prediction and unconventional natural gas exploration strategies. Practically, exploration should prioritize barrier island facies with evidence of mesodiagenetic dissolution (e.g., high secondary porosity >2.5%) and Type I/II throat signatures, using seismic facies mapping and targeted coring to optimize drilling in high-quality zones.

Conflicts of Interest

The authors declare no conflicts of interest regarding the publication of this paper.

References

Abdulhadi, D., Ali, J. A., & Hama, S. M. (2025). Advanced Techniques for Improving the Production of Natural Resources from Unconventional Reservoirs: A State-of-the-Art Review. *Energy Fuels, 39,* 10853–10876. https://doi.org/10.1021/acs.energyfuels.5c01259

Caineng, Z., Guangya, Z., Shizhen, T., Suyun, H., Xiaodi, L., Jianzhong, L. et al. (2010). Geological Features, Major Discoveries and Unconventional Petroleum Geology in the Global Petroleum Exploration. *Petroleum Exploration and Development, 37,* 129-145. https://doi.org/10.1016/S1876-3804(10)60021-3

Chen, X., Wang, T., Wu, S., Deng, Z., Li, J., Ren, Z. et al. (2024). Characterisation of the Full Pore Size Distribution of and Factors Influencing Deep Coal Reservoirs: A Case Study of the Benxi Formation in the Daning–Jixian Block at the Southeastern Margin of the Ordos Basin. *Processes, 12,* Article 2364. https://doi.org/10.3390/pr12112364

Congxian, L., & Ping, W. (1991). Stratigraphy of the late Quaternary Barrier–Lagoon Depositional Systems along the Coast of China. *Sedimentary Geology, 72,* 189-200. https://doi.org/10.1016/0037-0738(91)90011-2

Gao, H., & Wang, W. (2017). The Newly Discovered Yanchang Gas Field in the Ordos Basin, Central China. *Journal of Earth Science, 28,* 347–357. https://doi.org/10.1007/s12583-015-0661-5

Gao, J., Ma, B., Lu, Y., Zhang, W., & Cao, Q. (2022). Origin of Authigenic Kaolinite with Implications for Permian Tight Gas Sandstone Reservoirs in the Northern Ordos Basin, Central China. *Journal of Natural Gas Science and Engineering, 99,* Article 104429. https://doi.org/10.1016/j.jngse.2022.104429

Greentree, M. R., Li, Z., Li, X., & Wu, H. (2006). Late Mesoproterozoic to Earliest Neoproterozoic Basin Record of the Sibao Orogenesis in Western South China and Relationship to the Assembly of Rodinia. *Precambrian Research, 151,* 79-100. https://doi.org/10.1016/j.precamres.2006.08.002

Hu, C. L., Lin, Z. Q., Li, X., Quaye, J. A., & Fu, Z. Q. (n.d.). Tight Sandstone Reservoirs in Lacustrine Environments: Review and Perspectives. *International Geology Review, 2025,* 1-28.

Jia, A., Wei, Y., Guo, Z., Wang, G., Meng, D., & Huang, S. (2022). Development Status and Prospect of Tight Sandstone Gas in China. *Natural Gas Industry B, 9,* 467-476. https://doi.org/10.1016/j.ngib.2022.10.001

Kuang, L., Dong, D., He, W., Wen, S., Sun, S., Li, S. et al. (2020). Geological Characteristics and Development Potential of Transitional Shale Gas in the East Margin of the Ordos Basin, NW China. *Petroleum Exploration and Development, 47,* 471-482.

Leary, R. J., Umhoefer, P., Smith, M. E., Smith, T. M., Saylor, J. E., Riggs, N. et al. (2020). Provenance of Pennsylvanian-Permian Sedimentary Rocks Associated with the Ancestral Rocky Mountains Orogeny in Southwestern Laurentia: Implications for Continental-Scale Laurentian Sediment Transport Systems. *Lithosphere, 12,* 88-121. https://doi.org/10.1130/l1115.1

Li, B., Guo, Y., Hu, X., Wang, T., Wang, R., Chen, X. et al. (2025a). Pore Structure and Heterogeneity Characteristics of Deep Coal Reservoirs: A Case Study of the Daning–jixian Block on the Southeastern Margin of the Ordos Basin. *Minerals, 15,* Article 116. https://doi.org/10.3390/min15020116

Li, G., Wang, G., Feng, N., Chen, F., Feng, Y., Lu, C. et al. (2025b). Deep Coal-Rock Gas in China: A Review of Distribution, Geological Characteristics, and Its Enrichment Conditions. *ACS Omega, 10,* 23472-23491. https://doi.org/10.1021/acsomega.5c02056

Li, J., Wang, M., Li, Y., Yuan, K., Liu, L., & Meng, L. (2025c). Comparative Analysis of Microscopic Pore Throat Heterogeneity in the Chang 6 Tight Sandstone Reservoir: Implications for Production Dynamics and Development Strategies in the Wuqi-Dingbian Region, Ordos Basin. *Processes, 13,* Article 1109. https://doi.org/10.3390/pr13041109

Li, Y., Xu, L., Jing, Z., Wu, X., & Hu, W. (2023). Organic and Inorganic Geochemistry of Upper Paleozoic Marine-to-Continental Transitional Shales and the Implications for Organic Matter Enrichment, Ordos Basin, China. *Energy & Fuels, 37,* 18747-18771. https://doi.org/10.1021/acs.energyfuels.3c02761

Li, Y., Zhou, D. H., Wang, W. H., Jiang, T. X. et al. (2020). Development of Unconventional Gas and Technologies Adopted in China. *Energy Geoscience, 1,* 55-68. https://doi.org/10.1016/j.engeos.2020.04.004

Liu, H., Zhao, Y., Luo, Y., Chen, Z., & He, S. (2015). Diagenetic Facies Controls on Pore Structure and Rock Electrical Parameters in Tight Gas Sandstone. *Journal of Geophysics and Engineering, 12,* 587-600. https://doi.org/10.1088/1742-2132/12/4/587

Liu, S. (2023). Review of the Development Status and Technology of Tight Oil: Advances and Outlook. *Energy & Fuels, 37,* 14645-14665. https://doi.org/10.1021/acs.energyfuels.3c02726

Liu, Y., Liu, H., Jiao, Y. Q., & Zhao, J. H. (2024). Evolution and Uranium Mineralization of the Northern Ordos Basin Revealed by Detrital Zircons of the Jurassic Strata. *Geological Society of America Bulletin, 137,* 575-593. https://doi.org/10.1130/b37488.1

Ma, B., Lu, Y., Eriksson, K. A., Peng, L., Xing, F., & Li, X. (2021). Multiple Organic–Inorganic Interactions and Influences on Heterogeneous Carbonate-cementation Patterns: Example from Silurian Deeply Buried Sandstones, Central Tarim Basin, North-Western China. *Sedimentology, 68,* 670-696. https://doi.org/10.1111/sed.12797

Meissner, F. F., & Thomasson, M. R. (1999). Exploration Opportunities in the Greater Rocky Mountain Region, Central Western, U.S.A. *AAPG Bulletin, 83,* 12.

Meng, X., Pu, R., Dou, T., Liu, G., Gong, H., Song, M. et al. (2024). Longshore Changes in the Microfacies and Distribution of Clastic Barrier Coastal Sandbodies: A Case from the Benxi Formation in the Ordos Basin, China. *Journal of Petroleum Exploration and Production Technology, 14,* 1129-1148. https://doi.org/10.1007/s13202-024-01760-4

Mo, P., Luo, J., Mi, D., Chang, Z., Huang, H., Zhang, T. et al. (2021). Classification and Disintegration Characteristics of the Carboniferous Rocks in Guangxi, China. *Advances in Civil Engineering, 2021,* Article 8929808. https://doi.org/10.1155/2021/8929808

Pan, W., Jiang, Z., Fan, L., Zhang, Z., Li, Z., Ma, S. et al. (2024). Provenance of the He 8 Member of the Upper Paleozoic Shihezi Formation, Ordos Basin, China: Insights from Heavy Minerals, Paleocurrents, Detrital Zircon Chronology, and Hf Isotopes. *Minerals, 14,* Article 1076. https://doi.org/10.3390/min14111076

Wang, H., Ma, F., Tong, X., Liu, Z., Zhang, X., Wu, Z. et al. (2016). Assessment of Global Unconventional Oil and Gas Resources. *Petroleum Exploration and Development, 43,* 925-940. https://doi.org/10.1016/s1876-3804(16)30111-2

Wang, L., & Li, S. (2024). Geological Modeling of Shale Oil in Member 7 of the Yanchang Formation, Heshui South Area, Ordos Basin. *Applied Sciences, 14,* Article 6602. https://doi.org/10.3390/app14156602

Wang, X., Qiao, X., Mi, N., & Wang, R. (2019). Technologies for the Benefit Development of Low-Permeability Tight Sandstone Gas Reservoirs in the Yan'an Gas Field, Ordos Basin. *Natural Gas Industry B, 6,* 272-281. https://doi.org/10.1016/j.ngib.2018.11.017

Wang, Z., Liu, Y., Lu, S., Lin, L., Zhou, N., & Liu, Y. (2023). Differential Development Characteristics of Secondary Pores and Effects on Pore Structure and Movable Fluid Distribution in Tight Gas Sandstones in the Lower Permian, Northeastern Ordos Basin, China. *Geoenergy Science and Engineering, 224,* Article 211580. https://doi.org/10.1016/j.geoen.2023.211580

Whalen, M. T., & Day, J. E. (2010). Cross-Basin Variations in Magnetic Susceptibility Influenced by Changing Sea Level, Paleogeography, and Paleoclimate: Upper Devonian, Western Canada Sedimentary Basin. *Journal of Sedimentary Research, 80,* 1109-1127. https://doi.org/10.2110/jsr.2010.093

Wu, Y., Fang, X., & Ji, J. (2023). A Global Zircon U–Th–Pb Geochronological Database. *Earth System Science Data, 15,* 5171-5181. https://doi.org/10.5194/essd-15-5171-2023

Xi, K., Cao, Y., Jahren, J., Zhu, R., Bjørlykke, K., Zhang, X. et al. (2015a). Quartz Cement and Its Origin in Tight Sandstone Reservoirs of the Cretaceous Quantou Formation in the Southern Songliao Basin, China. *Marine and Petroleum Geology, 66,* 748-763. https://doi.org/10.1016/j.marpetgeo.2015.07.017

Xi, S., Liu, X., & Meng, P. (2015b). Exploration Practices and Prospect of Upper Paleozoic Giant Gas Fields in the Ordos Basin. *Natural Gas Industry B, 2,* 430-439. https://doi.org/10.1016/j.ngib.2015.09.019

Xiong, J., Zhang, P., Deng, C., Picotti, V., Liang, H., Ren, Z. et al. (2024). Neogene–Quaternary Channel Evolution and Provenance Shift of the Middle Yellow River. *Journal of Geophysical Research: Earth Surface, 129,* e2023jf007532. https://doi.org/10.1029/2023jf007532

Xu, X., Liu, L., Li, X., Yang, W., Cao, Y., Ma, H. et al. (2021). Sequence Stratigraphy, Sedimentary Characteristics of Barrier Coastal Sedimentary System of the Benxi Formation (Gaoqiao Area, Ordos Basin) and Favorable Reservoir Distribution. *Energy Reports, 7,* 5316-5329. https://doi.org/10.1016/j.egyr.2021.08.173

Yang, Y., Li, W., & Ma, L. (2005). Tectonic and Stratigraphic Controls of Hydrocarbon Systems in the Ordos Basin: A Multicycle Cratonic Basin in Central China. *AAPG Bulletin, 89,* 255-269. https://doi.org/10.1306/10070404027

Zhang, H., Guo, L., Wu, Z., & Ma, J. (2024). Pore-Throat Structure, Fractal Characteristics and Permeability Prediction of Tight Sandstone: The Yanchang Formation, Southeast Ordos Basin. *Scientific Reports, 14,* Article No. 27913. https://doi.org/10.1038/s41598-024-79203-7

Zhang, J., Shi, M., Wang, D., Tong, Z., Hou, X., Niu, J. et al. (2022). Fields and Directions for Shale Gas Exploration in China. *Natural Gas Industry B, 9,* 20-32. https://doi.org/10.1016/j.ngib.2021.08.014

Zhang, W., Shi, Z., & Tian, Y. (2020). An Improved Method to Characterize the Pore-Throat Structures in Tight Sandstone Reservoirs: Combined High-Pressure and Rate-Controlled Mercury Injection Techniques. *Energy Exploration & Exploitation, 38,* 2389-2412. https://doi.org/10.1177/0144598720920729

Zhao, Z., Xu, W., Zhao, Z., Yi, S., Yang, W., Zhang, Y. et al. (2024). Geological Characteristics and Exploration Breakthroughs of Coal Rock Gas in Carboniferous Benxi Formation, Ordos Basin, NW China. *Petroleum Exploration and Development, 51,* 262-278. https://doi.org/10.1016/s1876-3804(24)60022-4

Zhu, S., Cao, Y., Huang, Q., Yu, H., Chen, W., Zhong, Y. et al. (2024). Impact of Pore Structure on Seepage Capacity in Tight Reservoir Intervals in Shahejie Formation, Bohai Bay Basin. *Journal of Marine Science and Engineering, 12,* Article 1496. https://doi.org/10.3390/jmse12091496

Zou, C., Zhai, G., Zhang, G., Wang, H., Zhang, G., Li, J. et al. (2015). Formation, Distribution, Potential and Prediction of Global Conventional and Unconventional Hydrocarbon Resources. *Petroleum Exploration and Development, 42,* 14-28. https://doi.org/10.1016/s1876-3804(15)60002-7

Zou, C., Zhang, G., Yang, Z., Tao, S., Hou, L., Zhu, R. et al. (2013). Concepts, Characteristics, Potential and Technology of Unconventional Hydrocarbons: On Unconventional Petroleum Geology. *Petroleum Exploration and Development, 40,* 413-428. https://doi.org/10.1016/s1876-3804(13)60053-1